Journal of Crystal Growth ▮ (▮▮▮▮) ▮▮▮–▮▮▮

Contents lists available at SciVerse ScienceDirect

Journal of Crystal Growth

journal homepage: www.elsevier.com/locate/jcrysgro

Characteristics of ZnO thin films doped by various elements

S. Kahraman *, H.M. Çakmak, S. Çetinkaya, F. Bayansal, H.A. Çetinkara, H.S. Güder

Physics Department, Mustafa Kemal University, 31034 Hatay, Turkey

ARTICLE INFO

Article history:
Received 14 May 2012
Received in revised form
16 August 2012
Accepted 6 October 2012
Communicated by D.P. Norton

Keywords:
A1. Crystal structure
A2. Growth from solutions
B1. Oxides
B1. Semiconducting II–VI materials

ABSTRACT

We have investigated the effects of Al, K and Co dopant elements on the properties of ZnO thin films deposited by CBD method on glass substrates. Changing in morphology, structural parameters, ionization energies of impurity levels, absorption behavior and optical band gap values were investigated through scanning electron microscopy (SEM), X-Ray diffraction (XRD), resistance–temperature measurement (R–T) and ultraviolet–visible spectroscopy (UV–vis) techniques. From the SEM observations, various morphologies (rod-like, flower-like and rice-like) were observed. Those morphological variations were attributed to the change in stable growth mechanism of intrinsic ZnO, induced by different atomic radius and different electronegativity of dopants. XRD results indicated that all orientations are well indexed to hexagonal phase crystalline ZnO. The impurity level ionization energy values (ΔE) were estimated as 0.32/0.13/0.07 eV; 0.34/0.15 eV; 0.40/0.13 eV and 0.48/0.22 eV for the Al, K, Co doped samples and i-ZnO, respectively. Optical band gap values were found that the doped samples' were higher than the intrinsic one's. This increasing (blue shift) was attributed to a deterioration which occurred in the lattice of the structures after doping. This effect was also supported by the structural results.

1. Introduction

ZnO, due to its wide direct band gap (~3.3 eV), large exciton binding energy (60 meV), transparency in the visible range, non-toxicity, abundancy in nature, is an excellent versatile II–VI compound semiconductor [1–3]. ZnO nanostructures, as a II–IV binary semiconductor, have attracted considerable attention because of their good optical, electrical and easily tunable morphological properties and their potential applications in solar cells, solar energy-hydrogen conversion devices, photo-electrochemical hydrogen generation applications and sensors [4–7].However undoped ZnO thin films are not stable especially at high temperatures, doping the zinc oxide can reduce this disadvantage. Besides, that doping leads to an increase in the conductivity of the ZnO thin films [8]. The ZnO doping is achieved by replacing Zn^{2+} atoms with atoms of elements such as aluminum [9], potassium [10] and cobalt [11]. The fundamental properties of defects, which behave as interstitials and vacancies in the ZnO system, are still unsolved problems. However various defects induced by doping are often observed in ZnO, which result in defects in the fundamental properties of ZnO films [12]. Doping of nanorods to adjust the position of Fermi level of the semiconductor nanostructures may also be utilized to promote molecular adsorption onto the surface [13]. Many types of oxide compounds can be produced by several methods such as chemical bath deposition (CBD), sputtering, thermal evaporation, chemical vapor deposition and spray pyrolysis [11]. After all, CBD method, as a solution phase approach, is a promising, simple and effective technique because it is not necessary to feed power to the conductive substrates, as in electrochemical deposition, or to carry out the process in pressure vessels, as in hydrothermal synthesis. By CBD method, various nanostructures can be obtained simply by changing precursor chemicals, concentration of solution, growth temperature and growth time [14–16].In addition, the solution growth technology is suitable to obtain stoichiometrical ZnO films because of its oxygen-rich deposition environment [17].Many investigations are still carried out to improve the characteristics of ZnO materials. However, to the best of our knowledge, there is no study which compares the effects of Al, K and Co dopants on morphological, structural, electrical and optical properties of ZnO. Thus, it is of interest to us to investigate the influence of the Al, K and Co dopant elements on the properties of ZnO thin films deposited by CBD method. Changing in morphology, structural parameters like grain size, lattice strain and dislocation density, ionization energies of impurity levels, absorption behavior and optical band gap values were investigated.

2. Experimental procedure

In this study, microscope glass slides were used as substrate. The substrates were rinsed into dilute sulfuric acid solution (H_2SO_4:H_2O, 1:5, v/v) to remove native oxide layer, and then

* Corresponding author. Tel.: +90 326 245 5845; fax: +90 326 245 5867.
E-mail address: suleymanmku@gmail.com (S. Kahraman).

0022-0248/$ - see front matter © 2012 Elsevier B.V. All rights reserved.
http://dx.doi.org/10.1016/j.jcrysgro.2012.10.018

completely rinsed in acetone and double distilled water for 5 min prior to deposition of initial ZnO seed layer. After these treatments, substrates exhibit good hydrophilic property [18], which is vitally important to obtain uniform and continuous film layer. All the chemical materials used in the experiments were analytical grade. 0.1 M $Zn(NO_3)_2 \cdot 6H_2O$ was dissolved in distilled water and the initial pH value of the zinc nitrate solution was adjusted to ~10 by adding aqueous ammonia. 0.1 M $Al(NO_3)_3 \cdot 9H_2O$ (Molar mass: 375.134 g/mol), 0.1 M KNO_3 (molar mass: 101.1032 g/mol) and 0.1 M $Co(NO_3)_2 \cdot 6H_2O$ (molar mass: 291.03 g/mol) were added to each starting solutions as dopant sources at the concentration of 1 at%. Each complex solution was stirred for 20 min. Then, the previously cleaned glass substrates were immersed and the solutions were heated to 90 ± 1 °C. Heating rate was about 7 °C/min. Substrates were taken out from the bath after 20 min. For comparison, an intrinsic ZnO (i-ZnO) film was also deposited under the same conditions. Then, the samples were exposed to a heat treatment process at 640 K for 2 h to remove hydroxide phase included, if any. Surface morphology of each sample was observed using a scanning electron microscope (JEOL JSM-5500LV, Japan) with energy dispersive X-ray spectroscopy equipment (EDXS, Oxford Instruments ISIS 300). Structural analysis were carried out by using Philips X'pert Pro X-ray diffractometer (XRD) with Cu Kα radiation ($\lambda = 1.5418$ Å) at an operating voltage and current, 40 keV and 35 mA, respectively. Resistance–temperature characteristics of the structures were investigated by two point probe method in the temperature range of 300–723 K by using a Keithley 6487 interfaced with computer by a homemade Labview program. Optical absorption spectra in the UV–vis spectral range (200–1100 nm) of the structures were determined by using a UV–visible spectrophotometer (Hitachi U-1900).

2.1. Possible formation mechanisms of ZnO film

In the method used in this study, $[Zn(NH_3)_4]^{2+}$ complex is thermally decomposed in neutral aqueous solution and ions of Zn^{2+} and OH^- are released into solution. Finally $Zn(OH)_2$ or ZnO particles are formed. A dynamic equilibrium takes place in the precursor solution because of the presence of excessive ammonia. Two growth regimes are possible which are called homogeneous nucleation and heterogeneous nucleation during CBD process. In homogeneous nucleation mechanism; collisions occur between individual ions or molecules to form embryos which are nuclei that are intrinsically unstable against redissolution. Embryos grow by collecting individual species that collide with them. These embryos may re-dissolve in the solution before they have a chance to grow into stable particles (nuclei). On the other hand, in heterogeneous nucleation, subcritical embryos (or even individual ions) can adsorb onto the substrate. The energy required forming an interface between the embryo and the solid substrate will usually be less than that required for homogeneous nucleation, where no such interface exists. Therefore heterogeneous nucleation is energetically preferred over homogeneous nucleation and can occur near equilibrium saturation conditions, compared with the high degree of super-saturation often required for homogeneous nucleation [19].

CBD method is based on heating of alkaline zinc salt solution and precipitating of ZnO nanoparticles to the substrates. White precipitate of $Zn(OH)_2$ occurs when aqueous ammonia added to zinc nitrate solution. By adding excessive ammonia precipitate of $Zn(OH)_2$ dissolves. This can be represented by the following reactions [20]:

$$Zn(NO_3)_2 + 2NH_4OH \rightarrow Zn(OH)_2(s) + 2NH_4NO_3 \quad (1)$$

$$Zn(OH)_2(s) + NH_4OH \leftrightarrow (NH_4)ZnO_2^- + H_2O + H^+ \quad (2)$$

When the solution is heated, the ionic product exceeds the solubility product and precipitation occurs on the substrate and in the solution to form ZnO nuclei and thus ZnO film forms on the substrate by following reaction:

$$(NH_4)ZnO_2^- + H^+ \rightarrow ZnO + NH_4OH \quad (3)$$

3. Results and discussion

3.1. Surface morphology

Plain view SEM images of the intrinsic and doped ZnO samples are shown in Fig. 1. As seen clearly from Fig. 1a, i-ZnO sample is composed of dense, continuous and well-defined hexagonal shaped nanorods nearly perpendicular to the substrate surface.

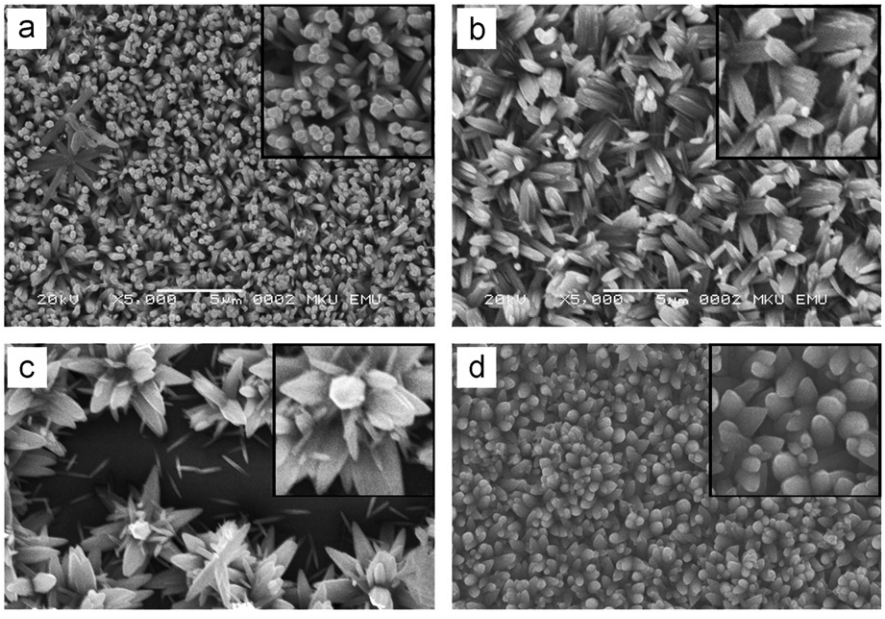

Fig. 1. Plain view SEM images of the intrinsic and doped ZnO samples (a) i-ZnO (b)–(d) Al, K and Co-doped ZnO samples, respectively.

Please cite this article as: S. Kahraman, et al., Journal of Crystal Growth (2012), http://dx.doi.org/10.1016/j.jcrysgro.2012.10.018

According to crystal growth mechanisms the growing faces of crystallites correspond to the crystal shape at equilibrium and are determined by the orientation of the crystal. A growth competition can start among the neighboring crystals according to their orientation. The faster growing crystals will grow over slower growing ones. Once the competition proceeds towards formation of same type of crystal faces, they form the free surface. This competitive growth mode represents an orientation selection resulting in the competitive growth texture [21–24]. For ZnO, stably preferential orientation is along to *c*-axis in rod shape. Usually, II–VI binary compound semiconductors crystallize in either cubic zinc blend or hexagonal wurtzite structure where each anion is surrounded by four cations at the corners of a tetrahedron, and vice versa. This tetrahedral coordination is typical of sp^3 covalent bonding nature. Thermodynamically stable phase of ZnO is wurtzite symmetry [1]. Fig. 1b–d shows SEM images of the doped ZnO samples with 1 at% Al, K and Co, respectively. From the figure, it can be seen that, the doping process deeply affects surface morphology of the structures and vertical alignment of the doped structures are lower than undoped one. Atomic radii of Al, K and Co are about 143, 227 and 125 pm, respectively while of Zn is 134 pm. Electronegativity of these elements are 1.61, 0.82 and 1.88, respectively. The evolving in morphologies may be related with different atomic radius and different electronegativity of dopants which affect the thermodynamically stable growth mechanism and free surfaces of the crystal faces of ZnO. In case of doping with Al (Fig. 1b), it can be seen that, individual hexagonal shaped rod-like structures are starting to merge with each other to form bundles and producing small clusters. In Fig. 1c, flower-like structures are seen and it can be said that the doping with potassium dramatically affects the growth behavior of ZnO. Potassium may decrease the nucleation rate in the solution, decrease the number of nuclei and then the growing can proceed via this lower amount of nuclei. It is well known that a decrease in number of seeds can cause randomly orientation which is the explanation of flower-like growth behavior in ZnO [25]. In case of Co (Fig. 1d), it can be seen that Co-doped ZnO sample is composed of denser and more aligned structures compare to the other ones. Owing to high electronegativity of Co (1.88), the effect suggested for the case of potassium doping may be acted adversely. As it will be seen in following section, XRD results support the above attributions for evolving in morphologies.

As a result, the morphological changes mentioned above may be related with the change in stable growth mechanism of the i-ZnO induced by different atomic radius and different electronegativity of dopants.

Energy dispersive spectra of the samples are shown in Fig. 2 and the compositional values are summarized in Table 1. The peaks corresponding to Si, Mg and Ca in Fig. 2c and d are coming from the glass substrate. The results in Table 1 prove that the doping process in our study is almost successful.

3.2. X-ray analysis

To investigate the effects of Al, K and Co dopants on structural properties of the samples, X-Ray diffraction patterns were obtained at an operating voltage and current, 40 keV and 35 mA, respectively. The 2θ range of 20°–70° was recorded at the rate of 0.02°.XRD patterns of the samples are shown in Fig. 3. The results indicated that all orientations were well indexed to hexagonal phase crystalline ZnO (wurtzite structure space group: $P6_{3mc}$(186); $a=0.3249$ nm, $c=0.5206$)(JCPDS 36–1451 card). The greater intensities of (002) peaks in respective patterns indicated that crystallites grow preponderantly oriented with *c*-axis normal to the substrate. This preferential growing feature was correlated

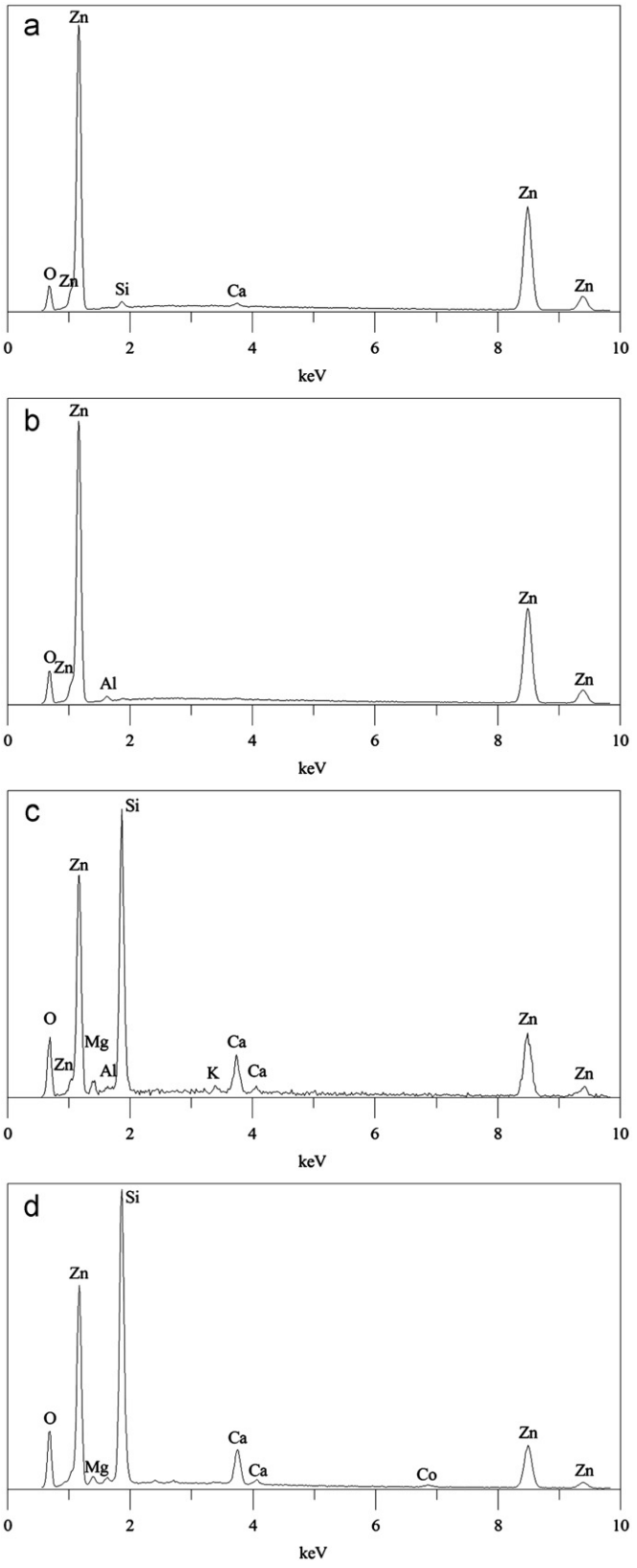

Fig. 2. EDX spectrum of the samples (a) i-ZnO, (b) Al–ZnO, (c) K–ZnO and (d) Co–ZnO.

with the self-ordering effect determined by the film trend to lower its surface energy during growth [26–28]. As it is shown in [26] the film grains, after their coalescence, grow mainly in the direction normal to the substrate surface. In the case of hexagonal

Table 1
Quantitative compositional analysis of the samples.

Composition (at%)	Sample			
	i-ZnO	Al–ZnO	K–ZnO	Co–ZnO
Zn	50	48.46	48.49	49.04
O	50	50.31	50.63	50
Dopant	–	1.23	0.88	0.96

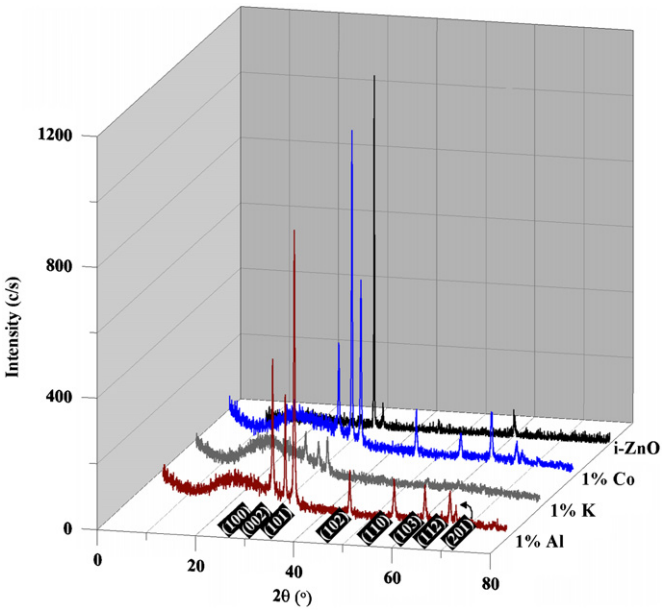

Fig. 3. XRD patterns of the samples.

crystalline structure, this direction will be [002] one. Most of the closely packed structures have the lowest free surface energy in the (002) plane. So crystallization favorably occurs in this direction. The average grain sizes (D) of the structures were calculated from the peak width at the half maximum of a peak (β), using Debye–Scherrer's equation [29]:

$$D = \frac{0.94\lambda}{\beta \cos\theta} \tag{4}$$

where λ is the wavelength of X-Ray radiation, θ is Bragg's angle of the peaks, and β is the angular width of peaks at FWHM. Each X-Ray diffraction peak obtained in a diffractometer is broadened due to instrumental and physical factors (grain size and lattice strains). All obtained and calculated structural parameters were summarized in the Table 2. As seen from the Table 2, grain sizes of the films were affected with doping elements.

To see the effects of dopant elements on some structural quantities of the films like microstrain (ε) and dislocation density (ρ), the following formulas were used [30]:

$$\varepsilon = \beta \cos\theta/4 \tag{5}$$

and

$$\rho = 15\varepsilon/aD \tag{6}$$

where a is lattice constant. From the table it can be seen that microstrain and dislocation density values increase after the doping process, indicating the deterioration in the lattice of i-ZnO. Additionally, it is obvious from the patterns that the doped samples have slightly higher 2θ values than the i-ZnO and the reference one. This kind of shift indicates the presence of increasing lattice strains in the structures [31]. In Bragg's formula ($2d \sin\theta = n\lambda$) it results that an increase of the inter-planar spacing, as consequence of the lattice strain which may be induced in the structure during preparation procedure by various factors as impurities, lattice defects, vacancies or deformation faults, implies a shift to lower Bragg angle [32].

3.3. Electrical measurements

To find electrical activation energies of the impurity levels, resistance–temperature characteristics of the samples have been carried out by two point probe method in the temperature range of 300–723 K by using a Keithley 6487 interfaced with a computer by a Labview program. Silver electrodes were painted on the deposited films achieve ohmic contact with them. Generally, ZnO structures without any additional doping exhibit n-type conduction due to the intrinsic defects, which are attributed to native defects such as the Zn interstitial atoms and the oxygen vacancies [33]. As may be shown from the solid-state theory of semiconductors [34,35], in case of a semiconductor with one or more impurity levels, the temperature dependence of dark electrical resistance is given by

$$R(T) = R_0 o e^{E_g/2kT} + \sum_{i=1}^{n} R'_{0,i} e^{\Delta E_i/kT} \tag{7}$$

In equation above, R_0 and $R'_{0,i}$ are constants, E_g is the thermal band gap energy, ΔE_i is the electrical activation energies of the impurity levels, k is the Boltzmann constant, and T is temperature. In the region of relatively lower temperatures, the overall conductivity of the semiconductor samples is dominated by the charge carriers generated by ionization of impurity levels (extrinsic conductivity), and thus the second term in Eq. (7) prevails in the R_T dependence. At sufficiently higher temperatures, on the other hand, the temperature dependence of conductivity is dominated by the band-to-band electronic transitions. Under such conditions, the charge carriers acquire enough thermal energy to make an inter-band transition (the intrinsic conductivity is "activated" at these temperatures) [35]. According to previous discussion, the two terms appearing in Eq. (7) may be treated independently in the corresponding temperature intervals. So in the graph of $\ln(R)$ vs. $1000/T$ a number of linear trends appear which indicate the forbidden band gap and a number of impurity levels (band gap states) in the forbidden band gap. But, for a semiconductor with wide forbidden band gap like ZnO, conductivity is dominated by the charge carriers generated by ionization of impurity levels in the studied temperature interval. Thus the second term in Eq. (7) prevails in the R_T dependence. The decrease of dark electrical resistance upon increase of temperature in the region of extrinsic conductivity (corresponding to the lower temperature interval) follows the equation:

$$R(T) = \sum_{i=1}^{n} R'_{0,i} e^{\Delta E_i/kT} \tag{8}$$

$\ln(R)$ vs. $1000/T$ graphs of the samples are shown in Fig. 4. As seen from Fig. 4, there are discretelinear regions mean that different impurity levels can be calculate for each sample. By using Eq. (8), ΔE can be easily written as

$$\Delta E = k \frac{d(\ln R(T))}{d(1/T)} \tag{9}$$

The impurity level ionization energy values were calculated from the slopes of $\ln(R)$ vs. $1000/T$ graphs. The obtained impurity level electrical activation energy (ΔE) values are found as 0.32/0.13/0.07 eV; 0.34/0.15 eV; 0.40/0.13 eV and 0.48/0.22 eV for the Al, K, Co doped samples and i-ZnO, respectively. Rahman et al. [36] reported Al-doped ZnO nanostructures and found

Table 2
Obtained and calculated structural parameters of the samples (D, grain size; ε, microstrain; ρ, dislocation density; d, inter-planar spacing).

hkl	Al–ZnO			K–ZnO			Co–ZnO			i-ZnO			ZnO (ref)	
	2θ (deg.)	FWHM (deg.)	d (Å)	2θ (deg.)	FWHM (deg.)	d (Å)	2θ (deg.)	FWHM (deg.)	d (Å)	2θ (deg.)	FWHM (deg.)	d (Å)	2θ (deg.)	d (Å)
(100)	32.268	0.9446	2.7743	32.171	0.9446	2.7825	32.220	0.9446	2.7783	31.317	–	2.7934	31.770	2.8143
(002)	34.913	0.6298	2.5699	34.869	0.6298	2.5730	34.923	0.6298	2.5692	34.017	0.0787	2.5871	34.422	2.6033
(101)	36.758	0.9446	2.4451	36.891	0.6298	2.4366	36.891	0.6298	2.4366	35.833	0.1968	2.4592	36.253	2.4759
(102)	48.051	0.6298	1.8935	–	–	–	48.058	0.9446	1.8933	47.167	0.2362	1.9062	47.539	1.9111
(110)	57.122	0.9446	1.6125	57.141	1.152	1.6107	57.102	0.6298	1.6130	–	–	1.6188	56.603	1.6247
(103)	63.383	0.9446	1.4675	–	–	–	63.352	0.9446	1.4681	62.408	0.576	1.4722	62.864	1.4771
(112)	68.447	1.152	1.3696	–	–	–	68.408	1.152	1.3703	–	–	1.3725	67.963	1.3782
D (nm)	10.81			11.26			11.49			37.21				
$\varepsilon \times 10^{-4}$	34.69			34.12			32.91			9.86				
$\rho \times 10^{15}$ (cm^{-2})	10.31			10.12			9.35			0.81				

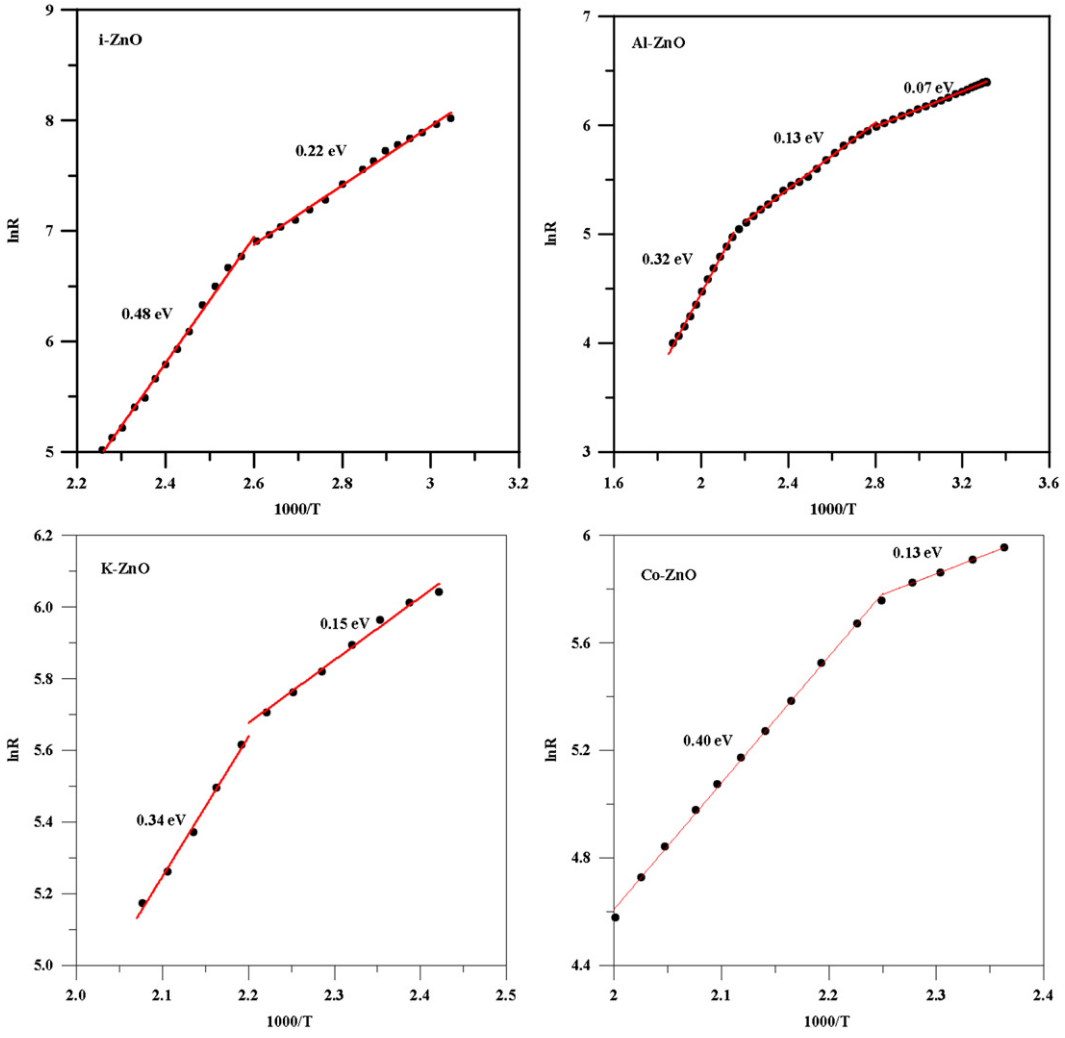

Fig. 4. ln$R$ vs. 1000/T graphs of the samples on the interval of 300–723 K.

0.32/0.40 eV and 0.21/0.24 eV for i-ZnO and 1% Al-doped ZnO structures. Mondal et al. [37] investigated the effect of Al incorporation on the activation energy of ZnO. They found the activation energies as 0.31 eV for both i-ZnO and Al–ZnO. No published data were found for the activation energy of K-doped ZnO. Nirmala et al. [38] reported (Mn,Co)-doped ZnO samples and found the activation energies as 0.40 eV and 0.80 eV for i-ZnO and (Mn,Co) co-doped ZnO, respectively. It can be seen that the activation energy values found in this study are well consistent with the literature values.

3.4. Optical measurements

Optical absorption spectra in the UV–vis spectral range (200–1100 nm) of the structures were determined using a UV–visible spectrophotometer. Fig. 5 shows the absorbance–wavelength

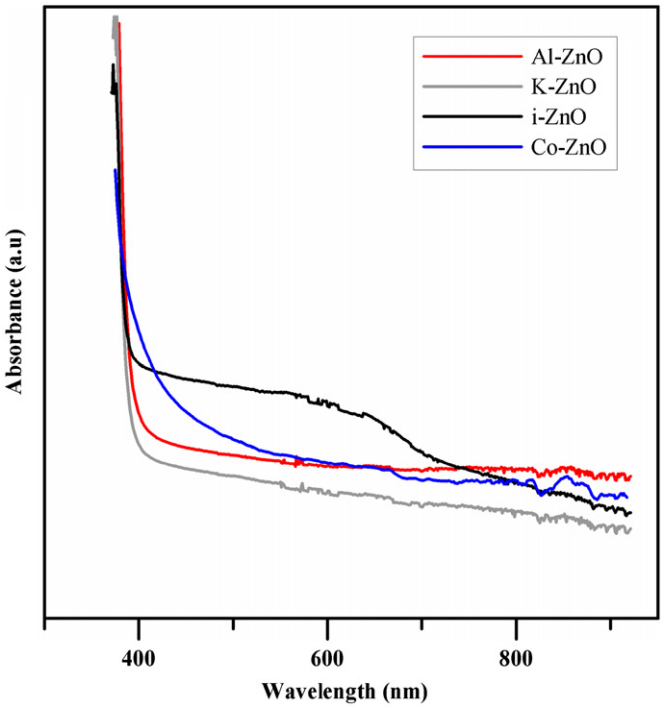

Fig. 5. Absorbance–wavelength relation of the samples in UV–vis range.

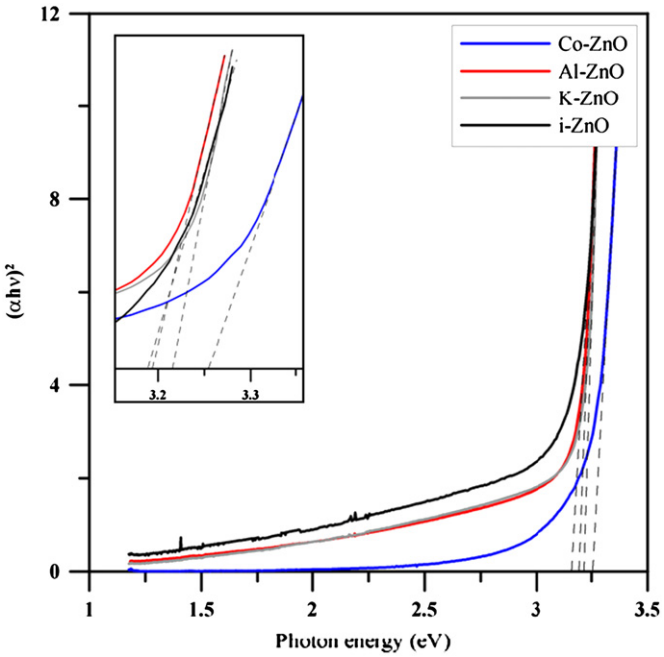

Fig. 6. Plots of $(\alpha h\nu)^2$ vs. photon energy, $(h\nu)$ of the samples.

relation of the samples. The analysis of the dependence of absorption coefficient on photon energy in the high absorption regions is performed to obtain the detailed information about the energy band gaps of the structures. The optical band gap of the structures is determined by the following relation [39].

$$(\alpha h\nu) = B(h\nu - E_g)^m \quad (10)$$

where B is an energy-independent constant, E_g is the optical band gap energy and m is an index that characterizes the optical absorption process and it is theoretically equal to 2 an 1/2 for indirect and direct allowed transitions, respectively. According to theoretical and practical results, ZnO exhibits direct inter-band transitions [40]. Thus we can choose m as 1/2. Plotting the graph of $(\alpha h\nu)^2$against photon energy$(h\nu)$, the band gap value can be determined by extrapolating the straight line portion.

Fig. 6 illustrates the plots of $(\alpha h\nu)^2$ vs. photon energy, $(h\nu)$ of the samples. From the Fig. 6, the E_g values were found about 3.19, 3.22, 3.25 and 3.18 eV for Al, K, Co doped ZnO and i-ZnO samples, respectively. It was seen that, E_g values of the doped structures were higher than the intrinsic one. This increasing which is caused by shifting of absorption edges to shorter wavelengths (blue shift) can be attributed to a deterioration which occurred in the lattices of the structures after doping. This effect was also supported by the structural results.

4. Conclusion

In this work, we have studied the influence of the Al, K and Co dopant elements on the properties of ZnO thin films deposited on glass substrates by CBD method. Changing in morphology, structural parameters like grain size, lattice strain and dislocation density, ionization energies of impurity levels, absorption behavior and optical band gap values were investigated.

- From the plain view SEM images of the samples, rod-like, flower-like and rice-like structures were observed. It was concluded that, doping process deeply affects surface morphology of the structures. Those morphological variations were attributed to the change in stable growth mechanism of intrinsic ZnO, induced by different atomic radius and different electronegativity of dopants. Atomic ratios in the intrinsic and doped samples were also supported with EDX measurements.
- The results indicated that all orientations are well indexed to hexagonal phase crystalline ZnO. It was seen that microstrain and dislocation density values in the samples increased after the doping process, indicating the deterioration in the lattice of i-ZnO.
- The impurity level ionization energy values of the samples were calculated from the slopes of ln$R$ vs. 1000/T graphs. The obtained impurity level electrical activation energy (ΔE) values were found as 0.32/0.13/0.07 eV; 0.34/0.15 eV; 0.40/0.13 eV and 0.48/0.22 eV for the Al, K, Co doped samples and i-ZnO, respectively.
- Optical band gap energy values of the samples were found about 3.19, 3.22, 3.25 and 3.18 eV for Al, K, Co doped ZnO and i-ZnO samples, respectively. It was found that, band gap values of the doped structures were higher than the intrinsic one. This increasing (blue shift) was attributed to a deterioration which occurred in the lattices of the structures after doping. This effect was also supported by the structural results.

In a future work, we will be focused to use the prepared structures for gas sensing applications and for solar cells as window layer.

Acknowledgments

This work was supported by Scientific Research Commission of Mustafa Kemal University (Project no: 1102 M 0101).

References

[1] H. Morkoç, Ü. Özgür, Zinc Oxide, Fundamentals, Materials and Device Technology, Wiley-VCH, Weinheim, 2009.
[2] C. Klingshirn, ChemPhysChem 12 (2007) 782.

[3] D.P. Norton, Y.W. Heo, M.P. Ivill, K. Ip, S.J. Pearton, M.F. Chisholm, T. Steiner, Materials Today 7 (2004) 34.
[4] B. Ergin, E. Ketenci, F. Atay, International Journal of Hydrogen Energy 34 (2009) 5249.
[5] F. Favier, E.C. Walter, M.P. Zach, T. Benter, R.M. Penner, Science 293 (2001) 2227.
[6] M. Seol, H Kim, W Kim, K Yong, Electrochemistry Communications 12 (2010) 1416.
[7] N.H. Al-Hardan, M.J. Abdullah, A. Abdul Aziz, International Journal of Hydrogen Energy 35 (2010) 4428.
[8] P. Nunes, E. Fortunato, P. Tonello, F.B. Fernandes, P. Vilarinho, R. Martins, Vacuum 64 (2002) 281–285.
[9] R.K. Shukla, A. Srivastava, A. Srivastava, K.C. Dubey, Journal of Crystal Growth 294 (2006) 427–431.
[10] M.K. Gupta, N. Sinha, B.K. Singh, B. Kumar, Materials Letters 64 (2010) 1825–1828.
[11] X.C. Liu, E.W. Shi, Z.Z. Chen, H.W. Zhang, L.X. Song, H. Wang, S.D. Yao, Journal of Crystal Growth 296 (2006) 135–140.
[12] Y. Zhao, M. Zhou, Z. Lv, Z. Li, J. Huang, X. Liang, J. Min, Materials Science in Semiconductor Processing 14 (2011) 257–260.
[13] A. Kolmakov, M. Moskovits, Annual Review of Materials Research 34 (2004) 151–180.
[14] F. Bayansal, F.H.A. Çetinkara, S. Kahraman, H.M. Çakmak, H.S. Güder, Ceramics International 38 (2012) 1859–1866.
[15] S. Kahraman, H.A. Çetinkara, F. Bayansal, H.M. Çakmak, H.S. Güder, Philosophical Magazine 92 (2012) 2150–2163, http://dx.doi.org/10.1080/14786435.2012.669064.
[16] F. Bayansal, S. Kahraman, G. Çankaya, H.A. Çetinkara, H.S. Güder, H.M. Çakmak, Journal of Alloys and Compounds 509 (2011) 2094.
[17] X.D. Gao, X.M. Li, W.D. Yu, Materials Research Bulletin 40 (2005) 1104.
[18] S. Kahraman, F. Bayansal, H.A. Çetinkara, H.M. Çakmak, H.S. Güder, Materials Chemistry and Physics 03 (2012) 108, http://dx.doi.org/10.1016/j.matchemphys.
[19] P. Suresh Kumar, A. Dhayal Raj, D. Mangalaraj, D. Nataraj, N. Ponpandian, Lin Li, G. Chabrol, Applied Surface Science 257 (2011) 6678.
[20] R. Saravana Kumar, R. Sathyamoorthy, P. Matheswaran, P. Sudhagar, Yong Soo Kang, Journal of Alloys and Compounds 506 (2010) 351.
[21] R.J. Hong, K. Helming, X. Jiang, B. Szyszka, Applied Surface Science 226 (2004) 378.
[22] H. Deng, J.J. Russell, R.N. Lamb, B. Jiang, Y. Li, X.Y. Zhou, Thin Solid Films 458 (2004) 43.
[23] Powder diffraction file 36-1451 for hexagonal Zinc Oxide, JCPDS-International Center for Diffraction Data, 1997.
[24] A. van der Drift, Evolutionary Selection, Philips Research Reports 22 (1967) 267.
[25] L. Vayssieres, International Journal of Nanotechnology 1 (2004) 1–41.
[26] T. Pauporte, D. Lincot, Electrochimica Acta 45 (2000) 3345.
[27] G. Hodes, Chemical Solution Deposition of Semiconductor Films, Marcel Dekker, Inc, New York, 2005.
[28] V.R. Shinde, C.D. Lokhande, R.S. Mane, S. Han, Applied Surface Science 245 (2005) 407.
[29] S.H. Jeong, B.N. Park, S.B. Lee, J.H. Boo, Surface and Coatings Technology 201 (2007) 5318.
[30] A. Suresh, K. Chatterjee, V. Sharma, S. Ganguly, K. Kargupta, D. Banerjee, Effect of pH on structural and electrical properties of electrodeposited Bi2Te3 thin films, Journal of Electronic Materials 38 (2009) 3.
[31] V. Pecharsky, P. Zavalij, Fundamentals of Powder Diffraction and Structural Characterization of Materials, Springer, New York, 2005.
[32] A. Suresh, K. Chatterjee, V. Sharma, S. Ganguly, K. Kargupta, D. Banerjee, Journal of Electronic Materials 38 (2009) 3.
[33] U. Ozgur, Y.I. Alivov, C. Liu, A. Teke, M.A. Reshchikov, S. Dogan, V. Avrutin, S.J. Cho, H. Morkoc, Journal of Applied Physics 98 (2005) 041301.
[34] K. Seeger, Semiconductor Physics, Springer, Berlin/Wien/New York, 1973.
[35] B. Pejova, A. Tanusevski, I. Grozdanov, Journal of Solid State Chemistry 178 (2005) 1786.
[36] M.M. Rahman, M.K.R. Khan, M. Rafiqul Islam, M.A. Halim, M. Shahja, M.A. Hakim, D.K. Saha, J.U. Khan, Journal of Materials Science and Technology 28 (2012) 329.
[37] S. Mondal, K.P. Kanta, P. Mitra, Journal of Physical Sciences 12 (2008) 221–229.
[38] M. Nirmala, P. Smitha, A. Anukaliani, Superlattices and Microstructures 50 (2011) 563–571.
[39] S. Ilıcan, M. Çağlar, Y. Çağlar, Applied Surface Science 256 (2010) 7204–7210.
[40] C.M. Muiva, T.S. Sathiaraj, K. Maabong, Ceramics International 37 (2011) 555–560.

Please cite this article as: S. Kahraman, et al., Journal of Crystal Growth (2012), http://dx.doi.org/10.1016/j.jcrysgro.2012.10.018